Magnetic nanodots from atomic Fe: Can it be done?

E. te Sligte†, R. C. M. Bosch, B. Smeets, P. van der Straten, H. C. W. Beijerinck, and K. A. H. van Leeuwen

Department of Applied Physics, Eindhoven University of Technology, P.O. Box 513, 5600 MB, Eindhoven, The Netherlands

Edited by Jack Halpern, University of Chicago, Chicago, IL, and approved February 7, 2002 (received for review October 5, 2001)

Laser focusing of Fe atoms offers the possibility of creating separate magnetic structures on a scale of 10 nm with exact periodicity. This can be done by using the parabolic minima of the potential generated by a standing light wave as focusing lenses. To achieve the desired 10-nm resolution, we need to suppress chromatic and spherical aberrations, as well as prevent structure broadening caused by the divergence of the incoming beam. Chromatic aberrations are suppressed by the development of a supersonic Fe beam source with speed ratio $S = 11 \pm 1$. This beam has an intensity of 3×10^{15} atoms sr^{-1} s^{-1}. The spherical aberrations of the standing light wave will be suppressed by aperturing with beam masks containing 100-nm slits at 744-nm intervals. The beam divergence can be reduced by application of laser cooling to reduce the transverse velocity. We have constructed a laser system capable of delivering over 500 mW of laser light at 372 nm, the wavelength of the $^5D_4 \rightarrow {}^5F_5$ atomic transition of ^{56}Fe we intend to use for laser cooling. Application of polarization spectroscopy to a hollow cathode discharge results in a locking system holding the laser continuously within 2 MHz of the desired frequency.

Laser focusing of atoms is being studied with increasing interest as it proves a viable technique to produce periodic nanostructures, especially because the period of the structures is known with great precision. The two basic lithographical processes are etching and deposition. Etching with the use of metastable rare gases, such as He* (1, 2), Ne* (3), and Ar* (4), as well as with alkali atoms like Na (5) and Cs (6) in combination with self-assembling monolayer (SAM) resists has produced arrays of lines and dots. Deposition of similar structures has been achieved with metal atoms such as Cr (1, 7, 8) and Al (9) and is being planned for other group III metals (10). The present work aims to deposit magnetic nanostructures made of Fe atoms. This method could provide a fascinating new experimental approach to the field of one- and zero-dimensional magnetism (11). For this scheme to work, we would have to deposit discrete, isolated structures of Fe.

Atom lithography is practiced in general by focusing atoms in the periodic potential created by a standing laser light wave, as depicted in Fig. 1. Atoms exposed to a nearly resonant light field experience a dipole force as a result of the electric field of the standing wave. This standing wave results in a sinusoidal potential. The ''sharpness'' of the focused image is determined in atom optics as in conventional optics by the incoming beam collimation and chromatic aberration. These two aspects are determined by the transverse and axial velocity spreads, respectively. A third factor, which causes the contrast of the image to be degraded (i.e., atoms are also deposited in between the focus positions), is that the potential is sine-shaped, and thus not purely parabolic. This effect is called spherical aberration in analogy with conventional optics. Having optimized the properties of the incoming atom flux, we are still limited by the surface diffusion and the growth pattern of the iron on the surface. We suspect that the effects of surface diffusion are restricted (i.e., an increase of the full width at half maximum of the deposited structures below 2 nm), provided the contrast of the image is good and the substrate material is chosen such that the mobility of Fe atoms on the substrate is low. The problem of surface diffusion is thus coupled with the problem of spherical aberration. All of these problems will have to be solved if an array of truly separate, nanometer-sized magnets is to be created.

Atom beam properties can be manipulated through laser cooling (12). In laser cooling, an atom absorbs photons and reemits them in a random direction. If the photons are part of a laser beam, they all have the same momentum and thus will transfer a net momentum to the atom. If the laser frequency is slightly below that of the transition, atoms moving along the direction of the laser will absorb fewer photons than atoms moving in the opposite direction because of the detuning induced by the Doppler effect. Two counterpropagating laser beams thus have the net effect of transversely cooling an atomic beam. Laser cooling normally requires a closed, two-level transition. The Fe atom has no closed two-level transition available for laser cooling. We attempt laser cooling via the $^5D_4 \rightarrow {}^5F_5$ transition, at a wavelength of 372 nm. The total ''leak'' in this transition is 1/243, i.e., when an atom is excited, there is a chance of 1 in 243 that it will not decay back to the ground state from where it came. If this occurs, we cannot apply any further laser cooling or focusing to the atom.

First, the chromatic aberration is reduced by decreasing the axial velocity spread. Zeeman slowing (6) cannot be applied in this case because that technique requires very large numbers of absorptions. Therefore, the atoms have to leave the source with a very narrow velocity distribution. Supersonic sources have such a characteristic narrow velocity distribution (13).

The second obstacle is the beam divergence. We intend to reduce the transverse velocity spread by transverse laser cooling (14), as shown schematically in Fig. 1. Our simulations show that a beam divergence of 0.2 mrad can be achieved in this way, whereas the atoms undergo less than 100 absorptions.

Third, we need to suppress the spherical aberrations resulting from the potential not being parabolic in most places. We intend to achieve this by means of the use of separately produced beam masks that block the beam in places except where the potential is harmonic in good approximation. This approximation is shown in Fig. 1.

This article aims to give an experimental overview of the progress made so far. We will begin by describing the design of our experiment in *Methods*. This description will be followed by a discussion of the operating characteristics of the experimental apparatus in *Results* and by a brief discussion of these results, as well as an outlook into the near future, in *Discussion*.

Methods

In this section, we give an overview of the design of our experiment. The three main components are a supersonic atomic

This paper results from the Arthur M. Sackler Colloquium of the National Academy of Sciences, ''Nanoscience: Underlying Physical Concepts and Phenomena,'' held May 18–20, 2001, at the National Academy of Sciences in Washington, DC.

This paper was submitted directly (Track II) to the PNAS office.

†To whom reprint requests should be addressed. E-mail: e.t.sligte@tue.nl.

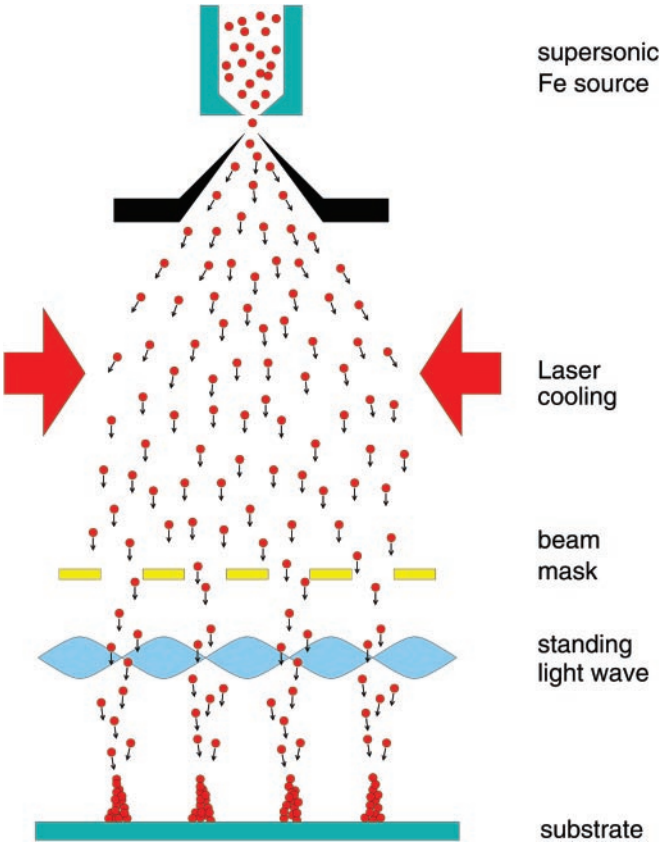

Fig. 1. Principle of Fe atom lithography. The Fe atoms exit a supersonic beam source. They are then collimated by laser-cooling techniques. After blocking of the unsuitable atoms by a beam mask, they will be focused in a periodic potential generated by a standing wave. We intend to use this scheme to create one- or zero-dimensional ferromagnetic nanostructures.

Fe source, a laser system capable of continuously generating over 500 mW of UV light, and beam masks with a periodicity to match the wavelength of the light used to focus the Fe atoms.

Beam Source. The source design reviewed in this section has been described more thoroughly by Bosch *et al.* (15). We use a design based on similar sources developed by Hagena (16).

The prime requirement of our source design is that the Fe atoms must have a uniform velocity distribution to reduce the chromatic aberrations in focusing. The uniformity of the velocity distribution is expressed in terms of the speed ratio S, defined as the ratio of the final flow velocity u and the parallel velocity spread $\alpha_{\|}$. This speed ratio is of the order unity for thermal sources; supersonic sources can have far greater speed ratios. We therefore use a supersonic source. Unfortunately, supersonic sources require inlet gas pressures of 10–10^4 mbar (millibar; 1 mbar = 100 Pa). Fe would require unrealistically high temperatures to have such a vapor pressure. We have therefore chosen to use Fe as a seed gas in a supersonic expansion of Ar.

With the use of a seeded supersonic source, we have drastically reduced the Fe vapor pressure required. We also demand that the Fe flux out of the source be sufficient to achieve a reasonable deposition rate. This rate can be achieved with operating temperatures around 2000 K. Several crucible designs have been tested, made of three different materials. High-density graphite turned out to dissolve in the liquid Fe. Boron nitride (BN) sources were corroded by the molten Fe. The only material that proved resistant to Fe and the high temperatures required was highly purified alumina (Al_2O_3), capable of withstanding temperatures up to 2200 K, its sublimation temperature. However, alumina is extremely hard and difficult to machine.

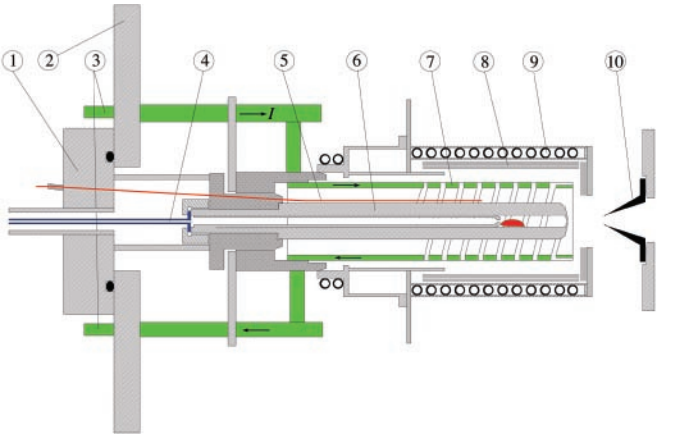

Fig. 2. Supersonic Fe atom source, with the oven and the gas source mounted on two separate flanges (*1* and *2*), along with copper connectors for the heating current (*3*). The Fe is seeded in a supersonic Ar expansion. The Ar flows into the source from a Ta gas inlet (*4*). A thermocouple (*5*) measures the temperature of the source. The source (*6*) is made of alumina and heated by a graphite heating coil (*7*). The oven is insulated by 20 layers of Ta foil (*8*) and its exterior is water-cooled (*9*). The beam is extracted from the source chamber by a skimmer (*10*).

The source currently in operation is depicted in Fig. 2. Because of the material it is made of, the crucible design has been kept extremely simple. Heating is applied externally by inserting the crucible into an oven, which consists of a doubly wound graphite heating coil. To prevent clogging, the last winding, located at the nozzle, has been made thinner: 1.5×5 mm^2 instead of 3×5 mm^2 for the other windings. Power losses are minimized by application of extensive heat shielding: 20 layers of tantalum foil around the circumference of the cylindrical oven and 5 layers at the nozzle side. A hole is left at the nozzle side to allow for expansion of the gas. Radiation through this hole is the dominant power loss process.

The alumina crucible itself consists of two parts, an inner tube and an outer tube. The Ar flows into the inner tube from the gas inlet. As it flows through the inner tube, it is heated to the source operating temperature. It leaves the inner tube through a 1-mm orifice, entering the source chamber. In the source chamber, the Fe vapor and the Ar gas mix. Upstream diffusion of Fe vapor into the source system is prevented by Ar flowing through the small space between the inner and outer tubes. The Ar/Fe mixture then exits through a nozzle 230 μm in diameter. This departure causes a supersonic expansion of the argon gas.

The argon expands into a chamber at 10^{-1} mbar; this pressure cannot be lower because of the large atomic flux into the chamber. Collision with the background gas causes the expansion to end in strong shock waves after 20–30 mm, called a Campargue expansion (17). To extract a steady beam from the source chamber, a conical skimmer is placed at a distance of 10–15 mm from the nozzle. The skimmer extracts part of the beam, which then expands into a far better vacuum (10^{-4} mbar) and does not encounter a shock front. The Fe in this beam will be used to deposit structures in a separate deposition chamber held at a background pressure of 10^{-8} mbar.

Laser System. For laser cooling and focusing of Fe, we estimate that a laser power of about 500 mW is necessary. There are no commercial systems capable of delivering 500 mW at 372 nm. To obtain light of the right wavelength, we have frequency-doubled a commercially available Ti:S laser operating at 744 nm by using a doubling system built at the Free University of Amsterdam.

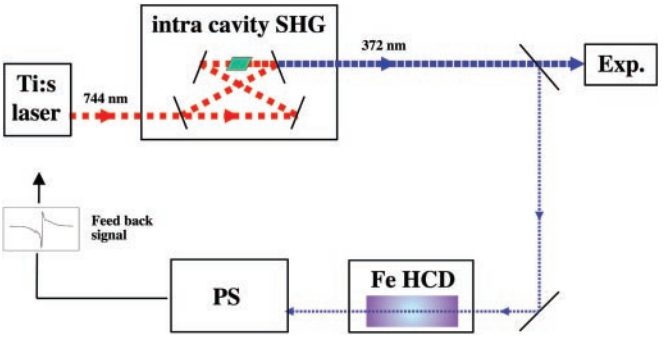

Fig. 3. The laser system to be used for laser-cooling of Fe. Laser light at 744 nm is generated in a tunable Ti:S laser. It is fed into a ring cavity with a lithium triborate crystal in it. In the crystal, light at 372 nm is generated through second harmonic generation (SHG), which can be used for laser cooling. A small portion of the laser light is diverted to a hollow cathode discharge (HCD) where polarization spectroscopy (PS) generates the error signal used to keep the laser tuned to the wavelength of the $^5D_4 \rightarrow {}^5F_5$ transition.

Frequency doubling is based on the nonlinear susceptibility of some materials. A full mathematical treatment (19) of the problem yields a quadratic dependence of second harmonic output power on the input power:

$$P_{2\omega} = K \times P_{\omega}^2 . \qquad [1]$$

The nonlinear crystal we use to obtain the second harmonic is lithium triborate (LBO). To maximize the power passing through the crystal, the crystal is placed in a ring cavity as shown in Fig. 3. The ring cavity consists of four mirrors, three with a reflection coefficient $R = 0.999$ and one with $R = 0.99$. The Ti:S laser light enters the cavity through the $R = 0.99$ mirror. The cavity length was locked to the incoming laser light wavelength with the use of the Pound–Drever–Hall technique (20). The finesse of the cavity was calculated at 469.

Having obtained the necessary output power at 372 nm, we need a way to lock the laser wavelength to the wavelength of the $^5D_4 \rightarrow {}^5F_5$ atomic transition. To do this, it is necessary to perform polarization spectroscopy on this transition (21). We need atomic Fe to observe this transition. In our setup, we generate the Fe atoms by sputtering from the cathode of a hollow cathode discharge. The discharge runs on He at 0.2 mbar; although this may seem a strange choice, because of the low sputtering probability for such a light element, it was chosen because other noble gases have relatively strong atomic transitions at or very near 372 nm. We applied polarization spectroscopy to this discharge. In polarization spectroscopy, Doppler broadening of the absorption profile is compensated for (21). This method theoretically enables us to obtain an error signal with a peak to peak width determined by the natural linewidth of the transition, $\Gamma/2\pi = 2.58$ MHz for our target transition. This laser system should enable us to successfully perform laser cooling and focusing of Fe.

Beam Masks. The potential induced by the standing light wave is a sine-type function. We intend only to use the near-parabolic minima and, to create structures with a zero background, block the rest of the potential. We intend to accomplish this with the use of beam masks. These beam masks would have holes or slits significantly less than half a wavelength-wide at a spacing of an integer number of wavelengths. The slit or hole dimension was chosen at 100 nm.

The thickness of the masks has to be on the order of the slit size for reasons of manufacturability. This means that the mask pattern has to be etched into a 100-nm thick membrane. The membrane is suspended on a section of Si wafer. The choice of material is limited by the fact that after deposition on Si, most materials are under an internal strain. This strain must not be compressive to prevent buckling and subsequent deformation of the grids. The tensile strain must also be small enough to prevent snapping of the structures, and the material itself must be stiff enough to prevent tensile deformation. The material that meets these criteria best is SiN (22, 23).

The masks are mounted on a section of standard Si[100] wafer. The etching of the pattern into the masks is done in two steps. First, the SiN film is covered with a resist layer. The desired pattern is etched into the resist layer by electron beam lithography. The second step is the actual etching itself of the SiN film by reactive ion etching. We expect the masks to allow sufficient suppression of spherical aberrations.

Table 1. Design parameters and standard operating conditions for the source

Supersonic source		
Operating temperature	T_0	300–2200 K
Ar inlet pressure	p_0	133–1600 mbar
Flow rate	$\dot{N}$	10^{19}–10^{20} s^{-1}
Nozzle diameter	d	0.2–0.25 mm
Skimmer diameter		0.5–0.8 mm
Nozzle–skimmer distance		10–15 mm
Beam attenuation parameter	q	$10.7 \cdot 10^{-4}$ $mbar^{-1}$

Results

We continue with a discussion of the operating properties of the parts of the setup completed thus far, starting with the atomic Fe beam source. We continue to discuss the laser system and the beam masks.

The robust source design used has lasted for over 2 years without noticeable deterioration. The crucible can operate without reloading for up to 200 h. The typical operating conditions of the source are summarized in Table 1. We have made a study of the properties of the Fe/Ar beam this source produces. The easiest way to determine the beam properties of an atomic Fe beam is by a time of flight method. We measured the intensity and velocity distribution of the Fe and Ar atoms with a mass spectrometer.

In determining the optimum expansion characteristics, we must take into account the imperfect extraction of the beam by the skimmer. The ideal center line argon beam intensity I_0^{id} in the supersonic expansion is known from fluid dynamics theory (13). As the flow passes through the skimmer, it is attenuated exponentially (18):

$$I_0 = I_0^{id} \cdot e^{-q \cdot p_0} , \qquad [2]$$

where q is the beam attenuation parameter, p is the operating pressure of the crucible, and I_0 is the actual center line beam intensity. This behavior has been measured by monitoring the argon mass spectrometer signal at varying source pressure, and thus q has been determined. The value found was $q = 10.7 \cdot 10^{-4}$ $mbar^{-1}$. The same value was found by measuring the Fe signal.

Given the Ar beam intensity and attenuation, there are two ways to deduce the iron beam intensity (15). One is to assume that the mass spectrometer detector sensitivity is the same for both species and multiply the Ar flux by the ratio of the Fe signal and the Ar signal. The other way is by multiplying the Ar flux with the ratio of the Fe and Ar source pressures. Both methods give results that agree to within a factor of 2. For both estimates, the Fe beam intensity lies between $I(0) = 10^{15} s^{-1} sr^{-1}$ and $I(0) = 10^{16} s^{-1} sr^{-1}$, depending on the operating conditions. The time of flight setup has also been used to measure the velocity distribution. The average velocity was $u = 1400$ m/s under standard

Table 2. Typical operating conditions and properties of the Ar–Fe beam

Operating characteristics		
Source temperature	T_0	1930 K
Ar inlet pressure	p_0	1050 mbar
Fe vapor pressure	p_v	0.1 mbar
Ar beam intensity	$I_{0,Ar}$	$2{\cdot}10^{19}$ s^{-1} sr^{-1}
Fe beam intensity	$I_{0,Fe}$	$3{\cdot}10^{15}$ s^{-1} sr^{-1}
Ar speed ratio	S_{Ar}	11
Fe speed ratio	S_{Fe}	11
Virtual source radius	R_v	0.25 mm
Beam divergence	R_v/z (z = 1 m)	0.25 mrad

operating conditions (see Table 2). The speed ratio was found to be $S = 11 \pm 1$ in this case.

The UV output power of the laser system critically hinges on the finesse of the cavity, which was determined from transmission measurements to be 177 ± 6. The cavity increases the laser power inside it by a factor of 90, and thus increases the 372-nm output power by a factor of 8100. The power output at 372 nm proved to depend quadratically on the input power into the cavity, with a conversion efficiency coefficient $K = 2.20 \pm 0.05 \times 10^{-4}$ mW^{-1}. This value enables the laser system to produce over 800 mW of 372-nm laser light if pumped with 2 W of red light. On a regular basis, 300 mW of light is produced at 1.4-W pump power.

The iron density and temperature inside the hollow cathode discharge were measured by absorption spectroscopy. The absorption dip had an FWHM of 1.00 GHz and an amplitude of about 40%. The temperature was deduced from the Doppler width of the absorption dip to be 673 ± 6 K. From the intensity of the absorption dip, the iron atomic density in the discharge was estimated at $3.2 \pm 0.2 \times 10^{16}$m^{-3}, corresponding to a partial Fe vapor pressure of 3×10^{-6} mbar. From our polarization spectroscopy setup, we obtained a dispersive error signal with a peak to peak width of 40 MHz. By using this error signal, we are able to keep our laser system in continuous lock within 2 MHz of the desired frequency.

The beam masks produced have a period of 744.2 ± 0.7 nm, twice the wavelength we intend to use. They have been made with a slit pattern as well as with a dot pattern. The lines are 100 ± 4-nm-wide, and the dots have a diameter of 100 ± 4 nm. The transmission masks cover a 250×250 μm area. An SEM picture of part of a sample beam mask for the deposition of lines is shown in Fig. 4.

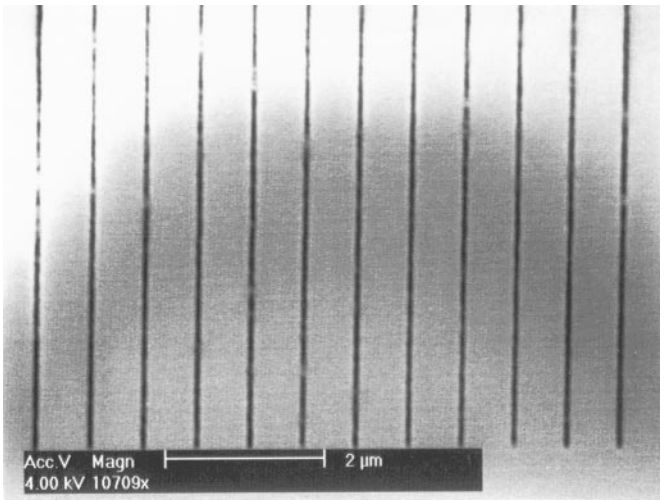

Fig. 4. SEM picture of a mask to be used for Fe line deposition. The lines are situated 744.2 ± 0.7 nm apart and are 100 ± 4-nm-wide.

Discussion

The values for average speed and speed ratio in the source expansion agree well with the values predicted by H.C.W.B. and Verster (13). The speed ratio is high enough to suppress chromatic aberrations in the focusing section to a minimum focus width of about 10 nm, sufficient to deposit the Fe nanostructures we aim to construct. The Fe beam intensity of at least 10^{15}s^{-1}sr^{-1} is sufficient to deposit nanostructures in a reasonable deposition time, and the speed ratio of around 11 is sufficient to effectively suppress chromatic aberrations.

Our laser system is capable of producing the 500 mW of continuous wave laser power needed and can be frequency-stabilized to within 1 line width. The difference between the theoretical and experimental value for the cavity finesse can be accounted for by stating that the calculation does not take into account absorption by the crystal and mirrors, and the possibility of imperfect transmission at the crystal faces. The 40-MHz-wide error signal (far greater than the predicted value of 2.58 MHz) can be explained with effects that increase the homogeneous linewidth, e.g., pressure broadening, Stark broadening, etc.

The design of the masks leaves two problems. One is the finite lifespan of the masks; we intend to deposit significant layers of iron, which will also be deposited onto the masks. The internal stresses of the iron film can cause the masks to deform or even break when the iron film thickness and mask thickness become comparable. This effect limits the lifetime of the masks to several depositions. An ample supply of masks has been produced, therefore this is no serious impediment to our experiments. The second problem is the alignment of the masks relative to the standing light wave. This alignment would have to be stable to about 10 nm. We plan to achieve this stability by monitoring the light scattered by the iron atoms in the standing light wave. The fluorescence will be minimal if the atoms passing through the slit traverse the standing light wave at the nodes. This scheme allows the position and the orientation of the mask with respect to the light wave to be adjusted and stabilized by using piezo-electric translators.

We conclude that currently our project has achieved three main results: an operational supersonic Fe beam source, an operational laser system delivering 500 mW of UV laser light, and beam masks that are ready for use. All three have been developed especially for this project. With the laser and Fe source operational, we have achieved laser cooling of Fe. To our knowledge, the laser cooling of Fe has never been done before.

We thank W. Hogervorst and coworkers at the Laser Lab of the Free University of Amsterdam for the design and construction of the frequency-doubling cavity. We also thank R. Navarro, M. F. A. Eurlings, and J. T. M. van Beek for design and production of the beam masks. This work is financially supported by the Dutch Foundation for Fundamental Research on Matter (FOM).

1. Brezger, B., Schulze, Th., Drodofsky, U., Stuhler, J., Nowak, S., Pfau, T. & Mlynek, J. (1997) *J. Vac. Sci. Technol.* **B15,** 2905–2911.
2. Petra, S. J. H., Feenstra, L., Vassen, W. & Hogervorst, W., International Quantum Electronics Conference/Conference on Lasers and Electron Optics, 12–14 September, 2000, Nice, France.
3. Engels, P., Salewski, S., Levsen, H., Sengstock, K. & Ertmer, W. (1999) *Appl. Phys. B* **69,** 407–412.
4. Berggren, K. K., Bard, A., Wilbur, J. L., Gillaspy, J. D., Helg, A. G., McClelland, J. J., Rolston, S. L., Phillips, W. D., Prentiss, M. & Whitesides, G. M. (1995) *Science* **269,** 1255–1257.
5. Timp, G., Behringer, R. E., Tennant, D. M. & Cunningham, J. E. (1992) *Phys. Rev. Lett.* **69,** 1636–1639.
6. Lison, F., Adams, H. K., Schuh, P., Haubrich, D. & Meschede, D. (1997) *Appl. Phys. B* **65,** 419–421.

7. McClelland, J. J., Scholten, R. E., Palm, E. C. & Celotta, R. J. (1993) *Science* **262,** 877–880.
8. Andersson, W. R., Bradley, C. C., McClelland, J. J. & Celotta, R. J. (1999) *Phys. Rev. A* **59,** 2476–2485.
9. McGowan, R. W., Giltner, D. & Lee, S. A. (1995) *Opt. Lett.* **20,** 2535–2537.
10. Rehse, S. J., McGowan, R. W. & Lee, S. A. (2000) *Appl. Phys. B* **70,** 657–660.
11. Himpsel, F. J., Ortega, J. E., Mankey, G. J. & Willis, R. F. (1998) *Adv. Phys.* **47,** 511–597.
12. Metcalf, H. J. & van der Straten, P. (1999) *Laser Cooling and Trapping* (Springer, Berlin).
13. Beijerinck, H. C. W. & Verster, N. F. (1981) *Physica* **111C,** 327–352.
14. Hoogerland, M. D., Driessen, J. P. J., Vredenbregt, E. J. D., Megens, H. J. L., Schuwer, M. P., Beijerinck, H. C. W. & van Leeuwen, K. A. H. (1996) *Appl. Phys. B* **62,** 323–327.
15. Bosch, R. C. M., Beijerinck, H. C. W., van der Straten, P. & van Leeuwen, K. A. H. (2002) *Eur. Phys. J. Appl. Phys.*, in press.
16. Hagena, O. F. (1991) *Z. Phys. D* **20,** 425–428.
17. Campargue, R. (1964) *Rev. Sci. Instrum.* **35,** 111–112.
18. Shen, Y. R. (1984) *The Principles of Nonlinear Optics* (Wiley, New York).
19. Drever, R. W. P., Hall, J. L. & Kowalski, F. V. (1983) *Appl. Phys. B* **31,** 97–105.
20. Demtröder, W. (1981) *Laser Spectroscopy, Basic Concepts, and Instrumentation* (Springer, Berlin).
21. Cardinale, G. F. & Tustison, R. W. (1992) *Thin Solid Films* **207,** 126–130.
22. Ekstrom, C. R., Keith, D. W. & Pritchard, D. E. (1992) *Appl. Phys. B* **54,** 369–374.
23. Beijerinck, H. C. W., van Gerwen, R. J. F., Kerstel, E. R. T., Martens, J. F. M., van Vliembergen, E. J. M., Smits, M. R. Th. & Kaashoek, G. H. (1985) *Chem. Phys.* **96,** 153–173.